Self-Assembling Aromatic Peptide Amphiphile Fibers for Multivalent Display of Enzymatically Linked Antigenic Proteins

Wakabayashi, Rie
Department of Applied Chemistry, Graduate School of Engineering, Kyushu University

Ghazian Dzaky, Syahid Fathullah
Department of Applied Chemistry, Graduate School of Engineering, Kyushu University

Higuchi, Ayato
Department of Applied Chemistry, Graduate School of Engineering, Kyushu University

Cui, Honggang
Department of Chemical and Biomolecular Engineering, and Institute for NanoBiotechnology, The Johns Hopkins University

他

出版情報：ACS Applied Materials & Interfaces. 17 (31), pp.44240-44248, 2025-07-23. American Chemical Society (ACS)
バージョン：

ACS APPLIED MATERIALS & INTERFACES

www.acsami.org
Research Article

Self-Assembling Aromatic Peptide Amphiphile Fibers for Multivalent Display of Enzymatically Linked Antigenic Proteins

Rie Wakabayashi,*,§ Ghazian Dzaky Syahid Fathullah,§ Ayato Higuchi, Honggang Cui, Kosuke Minamihata, Noriho Kamiya, and Masahiro Goto

Cite This: ACS Appl. Mater. Interfaces 2025, 17, 44240−44248

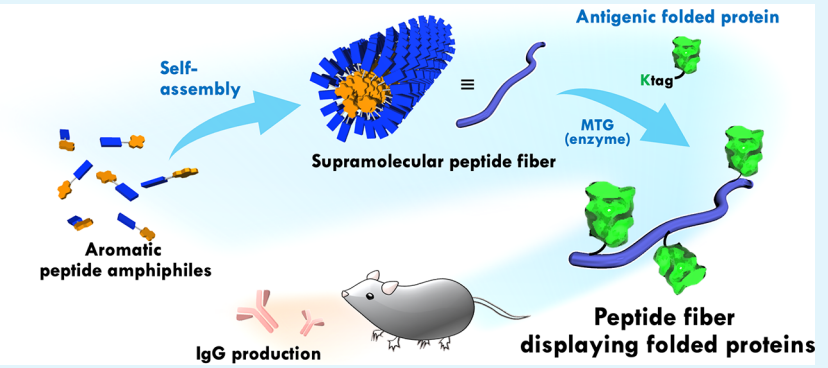

ABSTRACT: Supramolecular fibers assembled from peptide amphiphiles are promising materials for the delivery of biopharmaceuticals. However, strategies for directly conjugating folded proteins onto these supramolecular dynamic assemblies remain limited. Herein, we demonstrate that aromatic peptide amphiphiles that integrate self-assembly motifs with enzymatic recognition sequences enable the synthesis of supramolecular fibrous materials amenable to protein conjugation in their native folded state. The designed peptide amphiphiles self-assembled into fibers through a combination of hydrophobic, aromatic, and hydrogen bonding interactions in aqueous media. Using microbial transglutaminase, a recombinant enhanced green fluorescent protein (EGFP), used as a model proteinaceous antigen, was covalently coupled to the fibers via site-specific enzymatic cross-linking. This direct conjugation greatly enhanced the intracellular delivery of EGFP to murine dendritic cells in a manner dependent upon the peptide design. Notably, the resulting conjugates exhibited markedly increased immunogenicity compared to the protein alone, as evidenced by the elevated production of antigen-specific immunoglobulin G. These findings position the conjugated supramolecular fibers as a versatile platform for protein delivery and vaccine development.

KEYWORDS: *peptide amphiphiles, self-assembly, enzymatic reaction, intracellular protein delivery, immune material*

INTRODUCTION

Proteins and peptides in pharmaceutics are steadily attracting interest because their high target specificity and potency make them less likely to cause adverse effects compared with small-molecule drugs. Applications of such biopharmaceuticals include diabetes and cancer treatments, regenerative medicine, and vaccines. However, their instability in a biological environment and poor ability to cross biological membranes pose intrinsic challenges,[1] necessitating the development of biopharmaceutical delivery methods.[2−4] These involve genetic alteration by Fc[5] and peptide fusion;[6] synthetic modification with hydrophilic polymers[7] and lipids;[8] and use of drug carriers, such as polymer micelles,[9] liposome/lipid nanoparticles,[10] and supramolecular materials made from amphiphilic molecules.[11]

Supramolecular materials made by the self-assembly of peptide amphiphiles provide beneficial properties and design diversity with regard to drug delivery systems.[12−14] In addition to the initial hydrophobic collapse induced by hydrophobic groups, secondary structure formations of peptide moieties and/or other interacting motifs, such as electrostatic and aromatic interactions, influence the nanostructures and hierarchical architectures of the assembled materials. One of the most promising applications of such systems in biomedicine is the conjugation of peptidic ligands to make high-affinity supramolecular materials for the delivery and sustained release of protein drugs such as growth factors,[15]

Received: May 24, 2025
Revised: July 7, 2025
Accepted: July 7, 2025
Published: July 23, 2025

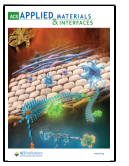

therapeutic enzymes,[16] and antibodies.[17] Another emerging example is the incorporation of antigenic peptides to produce immune materials.[18] Modulation in self-assembly motifs,[19] the secondary structures of peptide groups,[20] and the introduction of charged amino acids[21] reportedly influence the self-assembled structures and resultant bioactivities of these systems.

Although these peptidic ligands/epitopes can be easily coupled using synthetic approaches, few techniques allow direct, selective and efficient conjugation of correctly folded proteins. Strategies reported to date are limited to native chemical ligation,[22] active-site-directed conjugation,[23] split-protein approaches,[24] and enzymatic methods.[25−28] We have reported the enzymatic display of proteins on supramolecular fibers using microbial transglutaminase (MTG) from *Streptomyces mobaraensis*, an enzyme that catalyzes cross-links between the γ-carboxyamide of Gln residues and primary amines.[29] We previously demonstrated that 9-fluorenylmethoxycarbonyl-$(Leu)_n$-Gln-Gly (Fmoc-L*n*QG, n = 2, 3), an aromatic peptide amphiphile comprising both a self-assembly motif and MTG-reactive Gln residue, self-assembled into fibrous materials that could be postmodified with folded fluorescent proteins containing MTG-reactive primary amines.[26,27] The method is versatile because both the aromatic peptide amphiphiles and proteins to be displayed can be modified if the design criteria of self-assembly and enzymatic reactivity are satisfied. Moreover, because the displayed proteins retain their intrinsic structure and activity, the resultant supramolecular fiber−protein conjugates are good candidates for delivery of protein biopharmaceuticals.

To demonstrate this idea, we newly designed aromatic peptide amphiphiles, Pyr-L*n*QG (n = 2, 3), bearing a pyrenebutyryl (Pyr) group (Figures 1 and S1). The pyrenyl

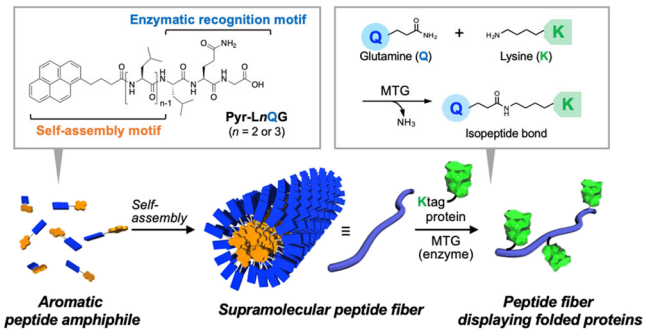

Figure 1. Chemical structure of aromatic peptide amphiphiles used in this study and schematic representation of the synthesis and modification of supramolecular fibers for delivery of protein biopharmaceuticals. Aromatic peptide amphiphiles containing an enzymatic recognition motif self-assemble into supramolecular fibers that react with microbial transglutaminase to conjugate and display folded proteins.

group has a large aromatic plane and is highly hydrophobic, which should enable formation of robust self-assembling structures[30,31] and serve as a fluorescent molecular probe in an aqueous environment.[32] Moreover, pyrenebutyrate has been demonstrated to enhance the direct cytosolic delivery of proteins conjugated to a cell penetrating peptide.[33] These properties make the pyrenebutyryl group a good candidate component of self-assembling molecules for protein delivery applications. Since Pyr-L*n*QG peptides contain an MTG-reactive Leu-Gln-Gly sequence, their self-assembly should yield supramolecular materials that can be postmodified with natively folded proteins via MTG catalysis (Figure 1). Direct conjugation to the supramolecular materials improved intracellular delivery to the immune cells, thereby enhancing the immunogenicity of the proteins displayed on their structures.

RESULTS AND DISCUSSION

Self-Assembly of Aromatic Peptide Amphiphiles. We first checked the self-assembly of Pyr-L*n*QG in pure water, citrate buffer, and phosphate buffer. A concentration of 1.0 mM Pyr-L*n*QG was used because surface tension and dynamic light scattering measurements suggested both Pyr-L2QG and Pyr-L3QG assemble at this concentration, their critical aggregation concentrations being ca. 65−70 and 15−35 μM, respectively (Figure S2). Fluorescence spectra of the Pyr-L2QG assembly were markedly dependent on the medium (Figure 2a, top). In pure water, fluorescence from the monomeric pyrene group at ca. 370−400 nm was dominant, while in citrate and phosphate buffers, emission at longer wavelengths became apparent, suggestive of excimer formation associated with aromatic−aromatic interactions between N-terminal pyrene groups.[34−36] The redshift was most pronounced in citrate buffer, with an emission maximum at ca. 480 nm. These suggest that the molecular packing/orientation is influenced by the buffer agents in Pyr-L2QG assembly. In contrast, fluorescence spectra of the Pyr-L3QG assembly in all three media were similar, with emission from the monomeric pyrene group being barely observed (Figure 2a, bottom). Fourier transform infrared (FT-IR) spectra were obtained to characterize interactions between peptides. The amide I (C=O stretching of amide group) and amide II (mainly N−H bending of amide group) absorbance bands were observed at 1632 and 1543 cm^{-1}, respectively, for both Pyr-L2QG and Pyr-L3QG (Figure 2b). While these bands were not clearly observed for those in citrate buffer due to the strong absorption from the carboxylate group of citrate ions, these results indicate that intermolecular hydrogen bonds were formed regardless of the number of Leu residues or assembly medium. These results contrast with the previously reported Fmoc-L*n*QG assemblies, in which hydrogen bond formation is highly influenced by the number of Leu residues.[26,27] This difference may stem from the linker between the aromatic pyrenyl group and the N-terminal amide group, which allows cooperative aromatic interactions and hydrogen bond formation. Transmission electron microscopy (TEM) showed that Pyr-L2QG and Pyr-L3QG assemblies had fibrous morphologies in all media. The density of Pyr-L2QG fibers depended on the medium, with the smallest number of fibers being formed in pure water and the densest network being observed in citrate buffer (Figure 2c). These observations suggest that the self-assembly of Pyr-L*n*QG peptides is mediated by aromatic interactions between pyrenyl groups and hydrogen bonding interactions between peptides. Moreover, in contrast with Fmoc-L*n*QG assemblies, the results suggest that these interactions are cooperative, each of them having a large impact on self-assembly of Pyr-L*n*QG.[26,27]

MTG-Catalyzed Conjugation of Folded Protein on Pyr-L*n*QG Fibers. We next investigated the reactivity of Pyr-L*n*QG fibers with MTG. As a model folded protein, we used an enhanced green fluorescent protein coupled with an MRHKGS hexapeptide (Ktag) as an MTG-reactive Lys residue to the C-terminus (Ktag-EGFP).[37] Ktag-EGFP (20 μM), MTG (0.3 U/

https://doi.org/10.1021/acsami.5c10222
ACS Appl. Mater. Interfaces 2025, 17, 44240−44248

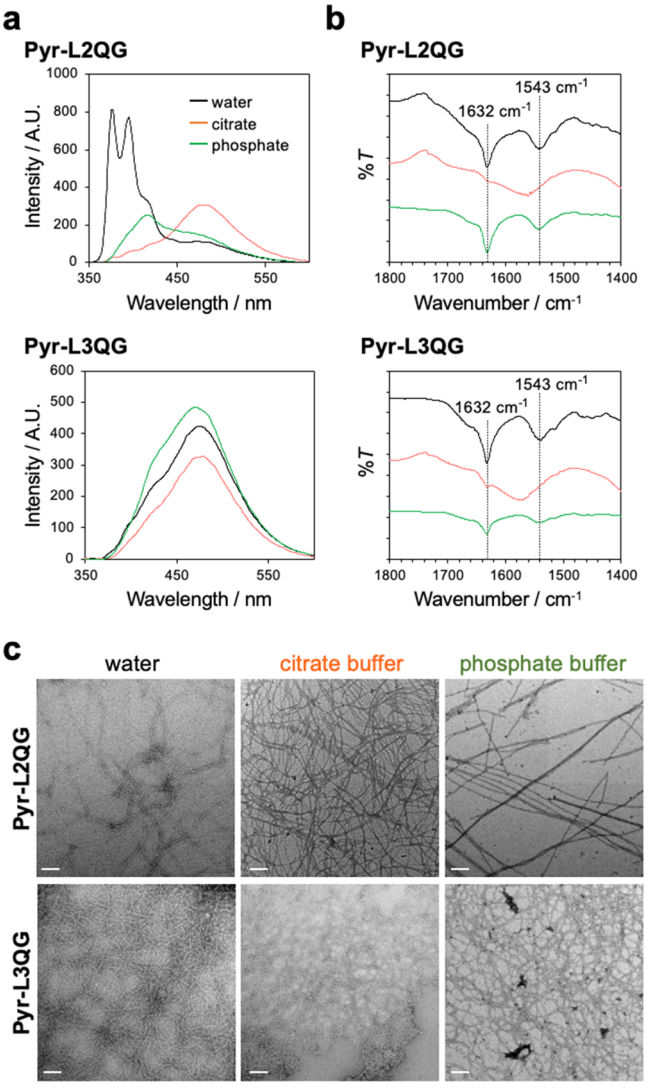

Figure 2. Pyrenebutyryl-$(Leu)_n$-Gln-Gly (Pyr-L*n*QG; n = 2, 3) peptides self-assemble into fibrous structures. (a) Fluorescence spectra (excitation wavelength, 340 nm). (b) Fourier transform infrared spectra. (c) Transmission electron micrographs. Pyr-L*n*QG peptides at a final concentration of 1.0 mM were prepared in pure water, citrate buffer (pH 6.5), and phosphate buffer (pH 6.5). Bars: 100 nm.

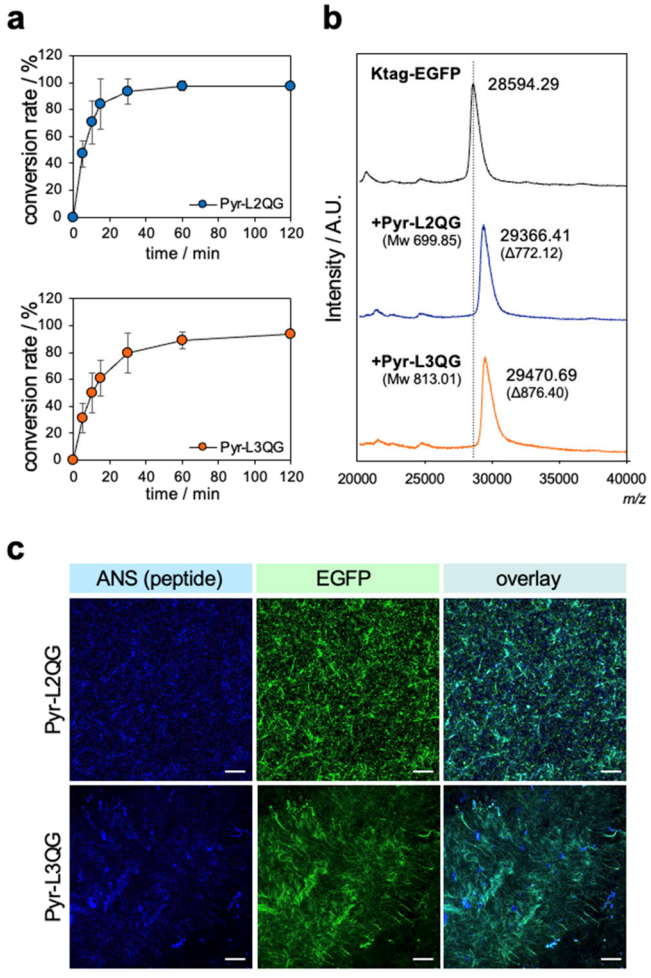

Figure 3. Enzymatic coupling of correctly folded enhanced green fluorescent protein (EGFP) to Pyr-L*n*QG fibers. (a) Time-course analysis of the reaction between an MRHKGS hexapeptide (Ktag) C-terminally conjugated to EGFP (Ktag-EGFP, 20 μM), Pyr-L*n*QG fibers (1.0 mM), and MTG (0.3 U/mL) at 37 °C. Data are mean ± SD (N = 3). (b) Matrix-assisted laser desorption/ionization-time-of-flight mass spectrometry analysis of Ktag-EGFP conjugated to Pyr-L*n*QG. An α-cyano-4-hydroxycinnamic acid matrix was used. (c) Confocal microscopy images of EGFP-functionalized Pyr-L*n*QG fibers stained with 8-anilino-1-naphthalenesulfonic acid. Bars: 10 μm.

mL), and peptide fibers preformed from Pyr-L*n*QG (1.0 mM) were combined, and the reaction was allowed to proceed at 37 °C in 10 mM phosphate buffer (pH 6.5). The 50:1 molar ratio of Pyr-L*n*QG and Ktag-EGFP was used to provide a space between proteins on the fibers. A buffer solution with a pH of 6.5 was used because this is within the compatible pH range of 6.0−7.5 for vaccine formulations.[38] High performance liquid chromatography (HPLC) analysis revealed that the enzymatic conjugation of Pyr-L*n*QG and Ktag-EGFP reached a plateau after 30 min under these reaction conditions (Figure 3a). Pyr-L2QG reached the plateau faster than Pyr-L3QG: Pyr-L2QG and Pyr-L3QG had conversion rates of ca. 93 and 79% at 30 min, respectively. The Fmoc-L*n*QG assemblies had a similar tendency, i.e., Fmoc-L2QG had faster and higher reactivity with regard to MTG catalysis than Fmoc-L3QG.[26,27,39] However, after 120 min, the reaction was confirmed to be >90% complete for both Pyr-L2QG and Pyr-L3QG assemblies.

Matrix-assisted laser desorption/ionization coupled with time-of-flight mass spectrometry (MALDI-ToF MS) showed shifts in m/z of 772.12 and 876.40 after conjugation of Ktag-EGFP to Pyr-L2QG and Pyr-L3QG, respectively (Figure 3b). These shifts are close to the relative molecular masses of Pyr-L2QG (699.85) and Pyr-L3QG (813.01), consistent with site-specific 1:1 conjugation of Pyr-L*n*QG to the Lys residue of Ktag. To further confirm this, the MTG-catalyzed reaction products of Ktag-EGFP and Pyr-L3QG were digested with trypsin and the resultant peptide fragments were analyzed. MALDI-ToF MS analysis of a reaction-specific HPLC fraction corresponded to a Pyr-L3QG conjugate with an HKGS peptide fragment of the Ktag region (Figure S3). No other new fractions appeared after the reaction. These results clearly demonstrate that the conjugation of Ktag-EGFP to Pyr-L*n*QG fibers took place between the Lys residue of Ktag and the Gln residue of Pyr-L*n*QG with high yields.

Confocal microscopy enabled the direct observation of the localization of Ktag-EGFP after the reaction with Pyr-L*n*QG

https://doi.org/10.1021/acsami.5c10222
ACS Appl. Mater. Interfaces 2025, 17, 44240−44248

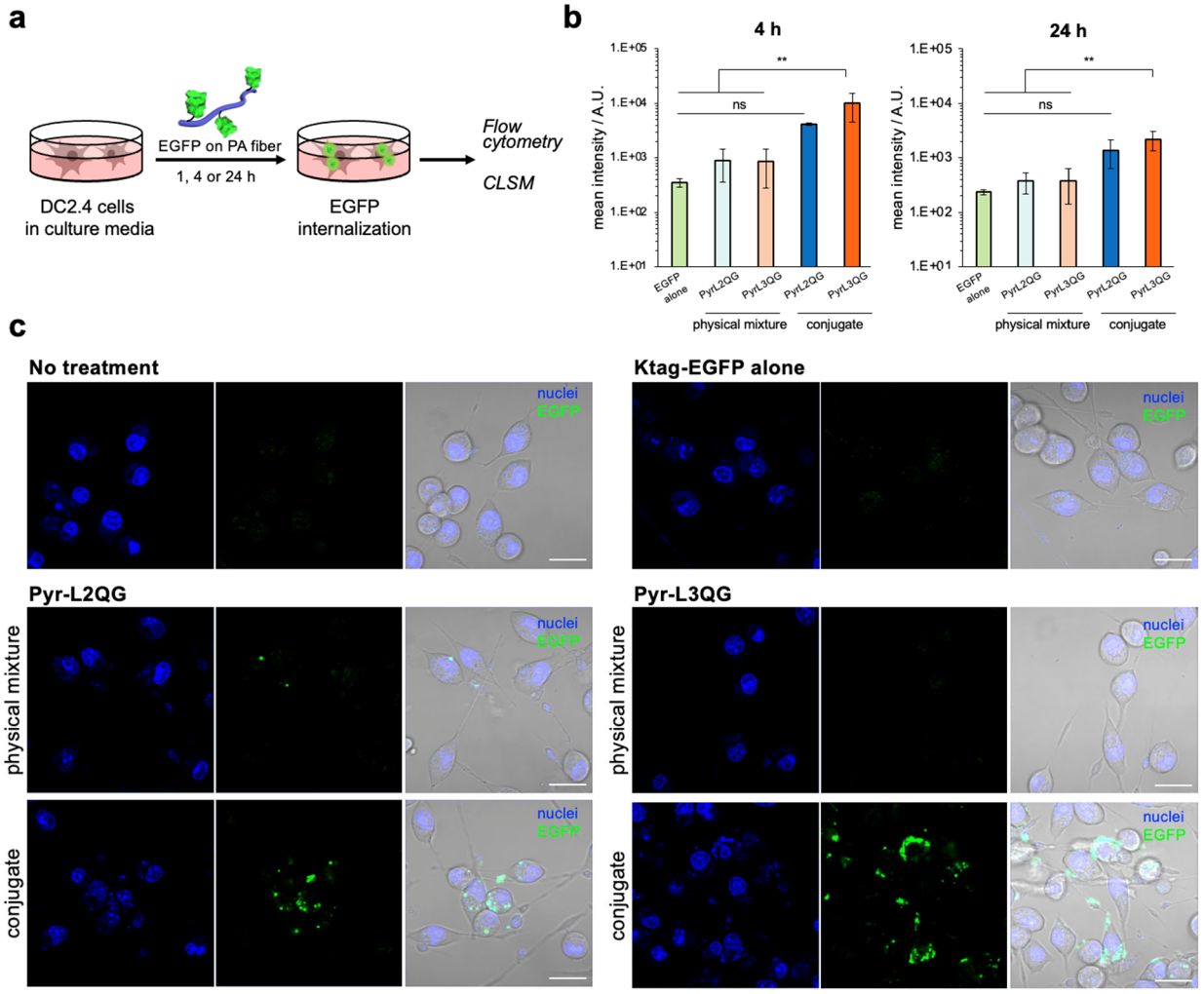

Figure 4. Delivery of Ktag-EGFP (Ktag = MRHKGS hexapeptide; EGFP = enhanced green fluorescent protein) to DC2.4 murine dendritic cells was enhanced by its covalent conjugation to Pyr-L3QG fibers. (a) Schematic illustration of the experiment. (b) Mean EGFP fluorescence intensities of DC2.4 cells treated with EGFP samples for 4 h (left) or 24 h (right). Data are mean ± SD (N = 3−4; ns, not significant; $^{**}p < 0.01$). (c) Localization of Ktag-EGFP delivered by various vehicles. DC2.4 cells were incubated with Ktag-EGFP alone, Ktag-EGFP conjugated to Pyr-L*n*QG fibers, or unconjugated mixtures of Ktag-EGFP and Pyr-L*n*QG fibers for 24 h, and then, the nuclei were stained with Hoechst 33342. Bars: 20 μm.

fibers[40] by staining the peptide fibers with 8-anilino-1-naphthalenesulfonic acid (ANS). Green fluorescence of Ktag-EGFP was colocalized with blue fluorescence of ANS bound to both Pyr-L2QG and Pyr-L3QG assemblies, suggesting that Ktag-EGFP specifically coupled to the fibrous structures without a loss of protein folding (Figure 3c). To examine if the Ktag-EGFP modification of the peptide influenced its assembly into fibers, fluorescence and FT-IR spectra were measured after the MTG reaction. In the former, fluorescence resonance energy transfer (FRET) from the pyrene excimer to EGFP was observed (solid lines in Figure S4a), indicating the close proximity of EGFP to Pyr-L*n*QG after the MTG reaction.[41] However, these FRET bands also appeared in unconjugated physical mixtures of Pyr-L*n*QG and Ktag-EGFP (dashed lines in Figure S4a). This might be explained by the physical entrapment of Ktag-EGFP in and/or on peptide assemblies mediated by nonspecific hydrogen bonding, electrostatic, and hydrophobic interactions, which are difficult to avoid.[42] The physical entrapment was also confirmed by direct observation by CLSM (Figure S5). The FRET ratio ($I_{\mathrm{EGFP,510\ nm}}/I_{\mathrm{Pyrene,435\ nm}}$) was almost identical for Pyr-L2QG before and after the MTG reaction. However, the ratio for Pyr-L3QG after the reaction was ca. 40% higher than that before the reaction (Figure S4b). Considering the reaction rates for Pyr-L2QG and Pyr-L3QG were almost identical (Figure 3a), this difference in FRET ratios may stem from the more oriented state of Ktag-EGFP proteins conjugated to Pyr-L3QG fibers, although the intrinsic mechanism remains unclear. FT-IR spectra of mixtures before and after the MTG reaction were the same, suggesting that the conjugation of Ktag-EGFP had little influence on the peptide assemblies (Figure S6). TEM images also revealed that morphologies of the supramolecular fibers remained after the conjugation of Ktag-EGFP, indicating their robustness (Figure S7).

In Vitro Delivery of Ktag-EGFP to Dendritic Cells. Intracellular delivery of Ktag-EGFP was investigated using the DC2.4 murine dendritic cell line. Along with the conjugated samples, free Ktag-EGFP and unconjugated mixtures of Ktag-EGFP and Pyr-L*n*QG fibers were used to examine the influence of the vehicle (Pyr-L*n*QG fibers) and the protein attachment mechanism (physical absorption vs chemical conjugation). Cells were added with each sample, incubated

https://doi.org/10.1021/acsami.5c10222
ACS Appl. Mater. Interfaces 2025, 17, 44240−44248

for 1 to 24 h, and then analyzed using flow cytometry (Figure 4a). The mean fluorescence intensity was compared among samples after 4 and 24 h incubation (Figure 4b). It is obvious that intracellular delivery of Ktag-EGFP was enhanced by its conjugation to Pyr-L*n*QG fibers, with ca. 12- and 28-fold greater delivery being measured after 4 h incubation with Pyr-L2QG and Pyr-L3QG conjugates, respectively, compared with Ktag-EGFP alone.

Interestingly, the enhanced Ktag-EGFP delivery was not observed in response to a mixture of unconjugated Ktag-EGFP and Pyr-L*n*QG, despite the apparent noncovalent entrapment of Ktag-EGFP in and/or on Pyr-L*n*QG peptide fibers (Figures S4 and S5). This result clearly demonstrates the necessity of direct chemical conjugation of proteins for their efficient intracellular delivery. Pyr-L3QG conjugates resulted in greater Ktag-EGFP delivery than Pyr-L2QG conjugates, possibly owing to the more oriented loading of Ktag-EGFP on Pyr-L3QG fibers, as discussed above, or more hydrophobic nature of Pyr-L3QG fibers. From these results, we can conclude that both the strategy of direct conjugation and the design of the peptide scaffolds to be conjugated are important factors determining the efficiency of protein delivery. Time-course flow cytometry investigation showed an initial increase (4 h) and then a decrease (24 h) in the mean fluorescence intensity (Figure S8, left). The decrease was most pronounced for Pyr-L*n*QG conjugates (Figure S8, right), suggesting that conjugated Ktag-EGFP was processed faster than unconjugated Ktag-EGFP. Consistent with the flow cytometry analysis, confocal fluorescence microscopy also identified a greater internalization of Ktag-EGFP after 4 h incubation of Pyr-L*n*QG conjugates compared with Ktag-EGFP alone (Figure S9). Importantly, Pyr-L3QG was less cytotoxic than Pyr-L2QG (Figure S10). Collectively, these findings show that supramolecular Pyr-L3QG fibers are a better protein carrier than Pyr-L2QG fibers.

Intracellular localization of Ktag-EGFP delivered to DC2.4 cells was also analyzed using confocal microscopy after 24 h. For cells treated with Ktag-EGFP alone and with unconjugated mixtures of Ktag-EGFP and Pyr-L*n*QG, EGFP fluorescence was barely detected, except in some cells treated with a mixture of unconjugated Ktag-EGFP and Pyr-L2QG (Figure 4c). In contrast, many bright green spots were observed inside the cells treated with Ktag-EGFP conjugated to Pyr-L*n*QG fibers, together with some large aggregates on cell surface. Internalization of the Pyr-L3QG conjugate decreased by ca. 72% when the cells were pretreated with NaN_3/2-deoxy-D-glucose to block cellular ATP synthesis (Figure S11), suggesting that the internalization of the conjugate is mainly an energy-dependent process. This was also confirmed by the subcellular localization of the Pyr-L3QG conjugate in lysosomes (Figure S12). We assume that the greater internalization of Pyr-L*n*QG conjugates of Ktag-EGFP compared with Ktag-EGFP alone may stem from the efficient accumulation of the conjugates on the cell surface, increasing the chance of phagocytosis.

In Vivo Vaccination Effect. Increased protein delivery to immune cells, i.e., DC2.4 cells, motivated us to further investigate conjugated materials for vaccine application. Supramolecular fibers displaying epitope peptides reportedly have self-adjuvanting effects, whereby the immunogenicity of the displayed epitopes is enhanced and no additional immunostimulant substances are needed to induce strong immune responses.[43] These supramolecular fibers are advantageous for design diversity and controllability, better recognition by immune cells owing to multivalent effects, and improved retention and controlled circulation in the body.[44]

The Pyr-L3QG conjugate was subcutaneously injected into the backs of C57BL/6N mice twice with a 2-weeks interval. Samples comprising Ktag-EGFP alone and a physical mixture of Ktag-EGFP and Pyr-L3QG were also used as controls. Blood samples were collected every 2 weeks and the levels of produced immunoglobulin G (IgG) in the sera were determined by enzyme-linked immunosorbent assays (ELISAs) (Figure 5A). The EGFP-specific IgG titer was

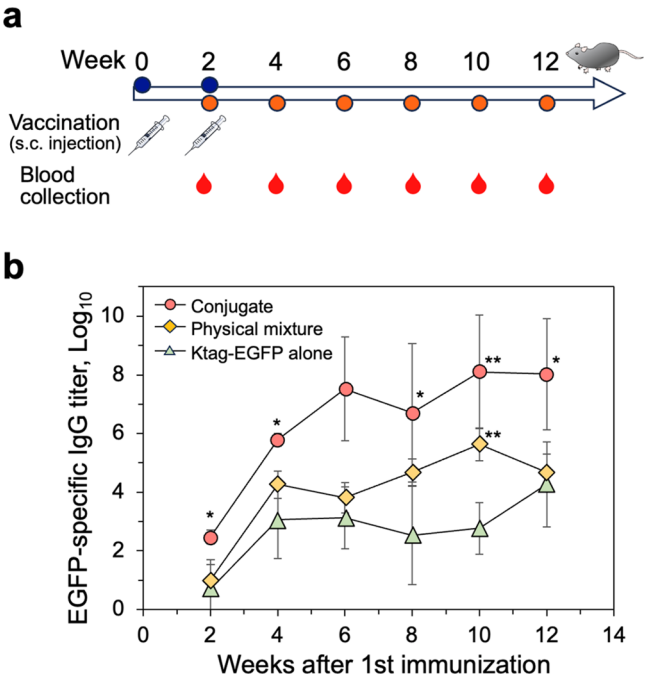

Figure 5. In vivo vaccination effect of Ktag-EGFP conjugated with Pyr-L3QG fibers (Ktag = MRHKGS hexapeptide; EGFP = enhanced green fluorescent protein). (a) Illustration of the experimental schedule. Blue and red markers in the schedule denote the vaccination and blood collection schedules, respectively. (b) EGFP-specific total IgG titer determined by enzyme-linked immunosorbent assay. Data are mean ± SD (N = 5; *p < 0.05, **p < 0.01 compared with Ktag-EGFP alone).

significantly higher with the Pyr-L3QG conjugate than with the protein alone at the very initial stage of the vaccination, i.e., 2 weeks after the first vaccination (Figure 5B). The IgG level continued to grow for 6 weeks. It was then either maintained or increased slightly until 12 weeks. The IgG level also increased in the mice injected with Ktag-EGFP alone up to 4 weeks. However, it remained similar after 4 weeks. Subclass analysis at 6 weeks indicated that the humoral immune response was induced by the Pyr-L3QG conjugate (Figure S13).

Importantly, the IgG level was much higher in the vaccination group with the Pyr-L3QG conjugate than in the physical mixture group, even though the component was the same, and the only difference was the method of antigenic protein attachment. Although some increase in the IgG level was observed for the physical mixture sample (at 10 weeks after the first immunization), the increased ratio was much higher with the Pyr-L3QG conjugate (an increase of ca. 70−3000-fold compared with Ktag-EGFP alone for the conjugate vs a 10−110-fold increase for the physical mixture during 2−

https://doi.org/10.1021/acsami.5c10222
ACS Appl. Mater. Interfaces 2025, 17, 44240−44248

12 weeks). These results clearly suggest that the increased immunogenicity caused by the Pyr-L3QG conjugate was not due to the copresence of the peptide fiber acting as an immunostimulant material, but was influenced by the direct attachment of the antigenic proteins to the peptide fiber. Although the close proximity of the proteins and fibers was suggested by the FRET experiment (Figure S4), the proteins may not have been in a coassembled state, in which they were able to demonstrate an adjuvanting effect,[45] but were rather in a weakly interacting state. Similar results have been reported for self-assembling, self-adjuvanting peptide fibers formed by Q11 peptide, βTail peptide,[46] helical peptide,[20] and lipid modification,[47] without marked inflammatory responses. In the present study, we used aromatic PAs composed of short 4−5 peptide sequences. They allowed us to make dramatic changes to the assembly mechanism, morphologies, and properties of the supramolecular fibers with a slight modification.[26,48] Further control over the immune responses might be enabled by modification, which is currently underway.

CONCLUSIONS

We have developed enzymatically active supramolecular peptide fibers and demonstrated their potential for intracellular protein delivery and vaccine applications. Aromatic peptide amphiphiles, Pyr-L*n*QG (n = 2, 3), self-assembled into supramolecular fibers via hydrophobic collapse, $\pi-\pi$ stacking interactions of pyrenyl groups, and hydrogen bonding between peptides backbones. These fibers were successfully functionalized with natively folded EGFP via a site-specific, MTG-mediated cross-linking reaction. The protein-fiber conjugates exhibited significantly enhanced uptake by murine dendritic cells compared to protein alone or a physical mixture of unconjugated protein and supramolecular fibers. Notably, EGFP conjugated to Pyr-L3QG fibers elicited substantially stronger humoral immune response, as evidenced by higher serum IgG levels, clearly demonstrating the advantage of covalent conjugation and supramolecular presentation in enhancing protein immunogenicity in vivo. Given the tunability of supramolecular fiber properties through peptide design, this platform offers a versatile and effective strategy for the controlled delivery of antigenic proteins and other protein-based therapeutics.

MATERIALS AND METHODS

Materials. Resins, amino acid/chemical reagents, and solvents for the synthesis of peptide amphiphiles were purchased from manufacturers and used as received. Fmoc-Gly-Alko-resin, Fmoc-Gln(Trt)-OH, Fmoc-Leu-OH, *O*-(1*H*-benzotriazol-1-yl)-*N*,*N*,*N*′,*N*′-tetramethyluronium hexafluorophosphate (HBTU), 1-hydroxy-1*H*-benzotriazole hydrate (HOBt), *N*,*N*-diisopropylethylamine (DIEA), piperidine, trifluoroacetic acid (TFA), and triisopropylsilane (TIS) were purchased from Watanabe Chemical Industries (Hiroshima, Japan). Acetonitrile (ACN), ammonium bicarbonate, dichloromethane, diethyl ether, dithiothreitol (DTT), iodoacetamide, methanol, HEPES, and 2-mercaptoethanol were obtained from Fujifilm Wako Pure Chemical Corporation (Osaka, Japan). Acetic acid (AcOH), citric acid, *N*-ethylmaleimide (NEM), *N*,*N*-dimethylformamide (DMF), sodium dihydrogen phosphate dihydrate, and urea were purchased from Kishida Chemical (Osaka, Japan). ANS and 1-pyrenebutyric acid were obtained from Sigma-Aldrich (St. Louis, MO, USA). Guanidine hydrochloride, trisodium citrate dihydrate, RPMI-1640 medium, antibiotic-antimycotic, and nonessential amino acids solution were purchased from Nacalai Tesque (Kyoto, Japan). Reagents for the Kaiser test were purchased from Kokusan Chemical Co. (Tokyo, Japan). Trypsin (sequencing grade, modified) was obtained from Roche (Basel, Switzerland).

Cell Culture. The murine dendritic cell line DC2.4 was obtained from Merck (SCC142). DC2.4 cells were grown in Roswell Park Memorial Institute 1640 medium supplemented with 10% v/v fetal bovine serum (Gibco), 10 mM HEPES, 50 μM 2-mercaptoethanol, 1× nonessential amino acids, and 1× antibiotic-antimycotic solution. The cells were cultured at 37 °C in a humidified atmosphere of 5% CO_2.

Animal Experiments. Female C57BL/6N mice (5−6 weeks old) were purchased from Kyudo (Saga, Japan) and maintained under standard conditions. All animal experiments were carried out with the authorization of the Ethics Committee for Animal Experiments of Kyushu University (approval no. A23-316-0) and in accordance with the Guide for the Care and Use of Laboratory Animals (Science Council of Japan).

Synthesis of Peptide Amphiphiles. Aromatic peptide amphiphiles, Pyr-L*n*QG (n = 2, 3), were synthesized using standard Fmoc-based solid-phase synthesis. Fmoc-Gly-Alko resin was immersed in dichloromethane and the Fmoc group was removed using 20% piperidine in DMF. A coupling reaction cocktail containing 3:3:3:6 mol equiv of Fmoc-protected amino acid/HBTU/HOBt/DIEA in DMF was added to one molar equivalent of resin in DMF and shaken for 1 h. After the repeated reactions involving Fmoc deprotection and peptide coupling, 1-pylenebutyric acid was coupled to the N-terminus. The aromatic peptide amphiphiles were cleaved from the resin using a mixture of 95% v/v TFA, 2.5% v/v TIS, and 2.5% v/v water for 1.5 h. After removing the solvents under reduced pressure, the peptides were precipitated and washed with cold diethyl ether. The crude peptide solids were purified using HPLC with an Inertsil ODS-3 column (GL Science, Tokyo, Japan) and a gradient of water and acetonitrile containing 0.1% v/v triethylammonium acetate. The fractions with each peptide amphiphile were collected, lyophilized, and stored at−20 °C until use. The purified peptides were analyzed using HPLC with an Inertsil ODS-3 column and using MALDI-ToF MS (autoflex maX, Bruker, Billerica, MA, USA) with an α-cyano-4-hydroxycinnamic acid (CHCA, Sigma-Aldrich) matrix.

Formation and Characterization of Self-Assembled Fibers of Aromatic Peptide Amphiphiles. Pyr-L*n*QG (n = 2, 3) powder was added to each aqueous medium (pure water, 10 mM citrate buffer, or phosphate buffer pH 6.5), dissolved by heating using a heat-gun, and allowed to cool to room temperature to form self-assembled fibers. For critical aggregation concentration (CAC) measurement, various concentrations of each sample were prepared in pure water, and the surface tension was measured using the pendant drop method with a drop shape analyzer DSA25 (KRUSS, Hamburg, Germany). The surface tension was recorded for 60 min, and the equilibrium surface tension, determined by averaging the values of the last 10 min, was plotted as a function of sample concentration to generate a CAC plot. Dynamic light scattering (Zetasizer Nano ZSP, Malvern Panalytical, Malvern, Worcestershire, UK) was also measured, and the light scattering intensity was plotted as a function of sample concentration. Fluorescence spectra of solution samples were recorded using an LS55 spectrometer (PerkinElmer, Waltham, MA, USA) with an excitation wavelength of 340 nm. For FT-IR spectral measurements, samples of self-assembled fibers were lyophilized and the solid powders were analyzed using a Spectrum Two spectrometer (PerkinElmer) in attenuated total reflectance mode. For TEM analysis, 3 μL of each sample was dropped onto a hydrophilized scanning TEM grid coated with an elastic carbon film (Okenshoji, Tokyo, Japan) and incubated for 1.5 min. The excess solution was then removed using filter paper, and the sample was stained with 2% w/v uranyl acetate solution for 2 min. TEM images were acquired using a JEM-2010 transmission electron microscope (JEOL, Tokyo, Japan) with an accelerating voltage of 120 kV.

Preparation of Ktag-EGFP and MTG. Ktag-EGFP[37] and MTG[49] were recombinantly expressed in *Escherichia coli* BL21 Star (DE3) as previously reported. The amino acid sequences of Ktag-EGFP and active MTG are shown below.

https://doi.org/10.1021/acsami.5c10222
ACS Appl. Mater. Interfaces 2025, 17, 44240−44248

Ktag-EGFP. MHHHHHHMVSKGEELFTGVVPIL-VELDGDVNGHKFSVSGEGEGDATYGKLTLK-FICTTGKLPVPWPTLVTTLTYGVQCFSRYPDHMKQHDFFK-SAMPEGYVQERTIFFKDDGNYKTRAEVKFEGDTLVNRIELK-GIDFKEDGNILGHKLEYNYNSHNVYIMADKQKNGIKVNF-KIRHNIEDGSVQLADHYQQNTPIGDGPVLLPDNHYLSTQ-SALSKDPNEKRDHMVLLEFVTAAGITLGMDELYRMRHKGS

MTG. SGGGGSDSDDRVTPPAEPLDRMPDPYRPSY-GRAETVVNNYIRWQQVYSHRDGRKQQMTEEQREWL-SYGCVGVTWVNSGQYPTNRLAFASFDEDRFKNELKNGRPRS-GETRAEFEGRVAKESFDEEKGFQRAREVASVMNRALENAHDE-SAYLDNLKKELANGNDALRNEDARSPFYSALRNTPSF-KERNGGNHDPSRMKAVIYSKHFWSGQDRSSSADKRKYGDP-DAFRPAPGTGLVDMSRDRNIPRSPTSPGEGFVNFDYGWFGAQ-TEADADKTVWTHGNHYHAPNGSLGAMHVYESKFRNWSE-GYSDFDRGAYVITFIPKSWNTAPDKVKQGWP

Conjugation of Ktag-EGFP and Peptide Fibers via MTG Catalysis. Ktag-EGFP (20 μM) and MTG (0.3 U/mL) were incubated with self-assembled Pyr-LnQG fibers (1.0 mM for confocal images or 200 μM for cellular experiments) in 10 mM phosphate buffer (pH 6.5) at 37 °C for 2 h. The reaction was terminated by adding NEM at a final concentration of 1 mM. The enzymatic conjugation rate at different time points was evaluated using a 1260 Infinity II HPLC system (Agilent Technologies, Santa Clara, CA, USA) with a Cosmosil 5Ph-AR-300 column (Nacalai Tesque, Kyoto, Japan) (4.6 mm × 150 mm) and a flow rate of 1.2 mL/min at 70 °C. A 33−53% gradient of ACN containing 0.1% v/v TFA was used over a 20 min period. The absorbance of protein-containing eluents was monitored at a wavelength of 380 nm. To determine the conjugation site, MALDI-ToF MS analysis of trypsin-digested peptide fragments was conducted. Specifically, fractions of free Ktag-EGFP and Ktag-EGFP conjugated to Pyr-L3QG were obtained and lyophilized. The solid samples were reconstituted in 200 μL of aqueous buffer containing 6 M guanidine hydrochloride, 100 mM ammonium bicarbonate, and 20 mM DTT and incubated at 60 °C for 90 min. To alkylate Cys residues, 16 μL of 0.5 M iodoacetamide was added, and the solution was then incubated at 60 °C for 60 min. The alkylated protein fractions were isolated using HPLC, lyophilized, and reconstituted in 50 μL of 100 mM ammonium bicarbonate buffer containing 8 M urea. To each solution, 150 μL of 20 μg/mL trypsin solution in 100 mM ammonium bicarbonate was added, and the digestion reaction was allowed to proceed at 37 °C for 2 h. Trypsin was then added, and the reaction was further conducted for 2 h. The digested peptide fragments were analyzed using HPLC with a Cosmosil $5C_{18}$-AR-300 column (4.6 mm × 150 mm) and a flow rate of 1.2 mL/min at 50 °C. A 5−50% gradient of ACN containing 0.1% v/v TFA was used over a 45 min period. The eluted peptide fragments were analyzed using MALDI-ToF MS (autoflex maX) in the reflector positive mode and a CHCA matrix.

For the direct observation of EGFP loaded on the peptide fibers, ANS was added at a final concentration of 100 μM, then the solution was drop-cast into a multiwell glass-bottom dish (Matsunami Glass Ind., Osaka, Japan) and imaged using an LSM700 confocal laser scanning microscope (Zeiss, Oberkochen, Germany) equipped with 405 and 488 nm diode lasers for observation of ANS and EGFP, respectively.

Intracellular Delivery of Ktag-EGFP to DC2.4 Cells. For flow cytometry analysis, DC2.4 cells (50,000 cells/well) were seeded in a 24-well plate and cultured for 24 h at 37 °C under a humidified 5% CO_2 atmosphere in RPMI-1640 medium (Nakalai Tesque) supplemented with 10% v/v FBS, 10 mM HEPES, 50 μM 2-mercaptoethanol, nonessential amino acids, and antibiotics. The cells were washed with Opti-MEM reduced serum medium (Thermo Fisher Scientific, MA, USA), then samples diluted 25-fold in Opti-MEM were added. After 1 or 4 h of incubation, samples were removed. The cells were washed with Opti-MEM and detached using accutase, and then the cell suspensions were analyzed using an Attune NxT flow cytometer (Thermo Fisher Scientific). For confocal images, DC2.4 cells (20,000 cells/well) were seeded in a multiwell glass-bottom dish and cultured for 24 h as above. The cells were washed with Opti-MEM, then samples diluted 20-fold in Opti-MEM were added. After 24 h of incubation, samples were removed. The cells were washed with Opti-MEM, stained with 2 μg/mL Hoechst 33342 for 10 min, then imaged using the LSM700 microscope with 405 nm (Hoechst 33342) and 488 nm (EGFP) diode lasers.

In Vivo Vaccination of C57BL/6N Mice. The C57BL/6N mice were randomly assigned to three groups and received s.c. injections of (i) Ktag-EGFP alone, (ii) Ktag-EGFP/Pyr-L3QG physical mixture, and (iii) Ktag-EGFP/Pyr-L3QG conjugate. The dose of Ktag-EGFP was set at 2 nmol of Ktag-EGFP (ca. 57 μg/mouse). Blood samples were collected from the tail veins every 2 weeks and serum was prepared. The Ktag-EGFP-specific IgG titer was evaluated by ELISA using a MaxiSorp immunoplate (Thermo Fisher Scientific) preabsorbed with Ktag-EGFP (1 μM, 100 μL/well). The peroxidase-conjugated secondary antibodies were antimouse IgG (H&L) (rabbit polyclonal, Rockland 610-4302), antimouse IgG1 (rabbit polyclonal, Rockland 610-4340), and antimouse IgG2c (goat polyclonal, SouthernBiotech 1078-05). The antibody titer was defined as the serum dilution factor at which the optical density became equal to that of the sera obtained prevaccination.

Statistical Analysis. GraphPad Prism 9 (GraphPad Software, La Jolla, CA, USA) was used for statistical analyses. For column analysis, significance was evaluated by one-way analysis of variance, followed by Tukey's post hoc test for multiple comparisons. For grouped analysis, two-way analysis was applied.

■ ASSOCIATED CONTENT

Supporting Information

The Supporting Information is available free of charge at https://pubs.acs.org/doi/10.1021/acsami.5c10222.

Characterization of Pyr-L*n*QG, critical aggregation concentration measurement, fluorescence, and FT-IR spectra; TEM images of peptide fibers after the conjugation of Ktag-EGFP; in vitro delivery of Ktag-EGFP; Pyr-L*n*QG cytotoxicity; inhibition of energy-dependent internalization of Ktag-EGFP; and subclass analysis of IgG produced in immunized mice (PDF)

■ AUTHOR INFORMATION

Corresponding Author

Rie Wakabayashi − *Department of Applied Chemistry, Graduate School of Engineering, Kyushu University, Fukuoka 819-0395, Japan;* orcid.org/0000-0003-0348-8091; Phone: +81 92 802 2809; Email: wakabayashi.rie.122@m.kyushu-u.ac.jp

Authors

Ghazian Dzaky Syahid Fathullah − *Department of Applied Chemistry, Graduate School of Engineering, Kyushu University, Fukuoka 819-0395, Japan*

Ayato Higuchi − *Department of Applied Chemistry, Graduate School of Engineering, Kyushu University, Fukuoka 819-0395, Japan*

Honggang Cui − *Department of Chemical and Biomolecular Engineering, and Institute for NanoBiotechnology, The Johns Hopkins University, Baltimore, Maryland 21218, United States;* orcid.org/0000-0002-4684-2655

Kosuke Minamihata − *Department of Applied Chemistry, Graduate School of Engineering, Kyushu University, Fukuoka 819-0395, Japan*

Noriho Kamiya − *Department of Applied Chemistry, Graduate School of Engineering, Kyushu University, Fukuoka 819-0395, Japan;* orcid.org/0000-0003-4898-6342

Masahiro Goto − *Department of Applied Chemistry, Graduate School of Engineering, Kyushu University, Fukuoka 819-0395, Japan;* orcid.org/0000-0002-2008-9351

Complete contact information is available at: https://pubs.acs.org/10.1021/acsami.5c10222

Author Contributions

§R.W. and G.D.S.F.: equally contributed.

Funding

This study was funded by the Japan Society for the Promotion of Science (JSPS) KAKENHI grants (JP25K01595, JP22H01884, and JP21H05227) and JSPS Bilateral Program Number JPJSBP120243507. R.W. thanks the Naito Foundation, Uehara Memorial Foundation, NOVARTIS Foundation (Japan) for the Promotion of Science, and Iketani Science and Technology Foundation, and The Kurata Grants by The Hitachi Global Foundation for financial support.

Notes

The authors declare no competing financial interest.

■ ACKNOWLEDGMENTS

R.W. thanks the Initiative for Realizing Diversity in the Research Environment for funding support. A.H. is grateful to the JSPS Research Fellowship for Young Scientists (Grant No. JP22KJ2482) and System Molecule System Device Da Vinci Course in Kyushu University for the scholarship. We thank the Advanced Research Infrastructure for Materials and Nanotechnology in Japan (ARIM) program of the Ministry of Education, Culture, Sports, Science, and Technology (MEXT) and the Center for Advanced Instrumental and Educational Support, Faculty of Agriculture, Kyushu University for facility support. We also thank Dr. Michio Kimura, Ms. Yuki Nabae, Mr. Tanaka, Mr. Sumi, and Dr. Ryo Sato (Kyushu University) for their assistance with experiments and fruitful discussions. We thank Frank Kitching, MSc., from Edanz (https://jp.edanz.com/ac) for editing a draft of this manuscript.

■ ABBREVIATIONS

MTG, microbial transglutaminase; FT-IR, Fourier transform infrared; TEM, transmission electron microscopy; EGFP, enhanced green fluorescent protein; HPLC, high-performance liquid chromatography; FRET, fluorescence resonance energy transfer

■ REFERENCES

(1) Mitragotri, S.; Burke, P. A.; Langer, R. Overcoming the Challenges in Administering Biopharmaceuticals: Formulation and Delivery Strategies. *Nat. Rev. Drug Discovery* **2014**, *13* (9), 655−672.

(2) Bizeau, J.; Mertz, D. Design and Applications of Protein Delivery Systems in Nanomedicine and Tissue Engineering. *Adv. Colloid Interface Sci.* **2021**, *287*, No. 102334.

(3) Moncalvo, F.; Martinez Espinoza, M. I.; Cellesi, F. Nanosized Delivery Systems for Therapeutic Proteins: Clinically Validated Technologies and Advanced Development Strategies. *Front. Bioeng. Biotechnol.* **2020**, *8*, 89.

(4) Srivastava, S.; Sharma, V.; Bhushan, B.; Malviya, R.; Awasthi, R.; Kulkarni, G. T. Nanocarriers for Protein and Peptide Delivery: Recent Advances and Progress. *J. Res. Pharm.* **2021**, *25* (2), 99−116.

(5) Levin, D.; Golding, B.; Strome, S. E.; Sauna, Z. E. Fc Fusion as a Platform Technology: Potential for Modulating Immunogenicity. *Trends Biotechnol.* **2015**, *33* (1), 27−34.

(6) Behzadipour, Y.; Hemmati, S. Considerations on the Rational Design of Covalently Conjugated Cell-Penetrating Peptides (CPPs) for Intracellular Delivery of Proteins: A Guide to CPP Selection Using Glucarpidase as the Model Cargo Molecule. *Molecules* **2019**, *24* (23), 4318.

(7) Pfister, D.; Morbidelli, M. Process for Protein PEGylation. *J. Controlled Release* **2014**, *180* (1), 134−149.

(8) Menacho-Melgar, R.; Decker, J. S.; Hennigan, J. N.; Lynch, M. D. A Review of Lipidation in the Development of Advanced Protein and Peptide Therapeutics. *J. Controlled Release* **2018**, *2019* (295), 1−12.

(9) Cabral, H.; Miyata, K.; Osada, K.; Kataoka, K. Block Copolymer Micelles in Nanomedicine Applications. *Chem. Rev.* **2018**, *118* (14), 6844−6892.

(10) Le Saux, S.; Aubert-Pouëssel, A.; Mohammed, K. E.; Martineau, P.; Guglielmi, L.; Devoisselle, J.-M.; Legrand, P.; Chopineau, J.; Morille, M. Interest of Extracellular Vesicles in Regards to Lipid Nanoparticle Based Systems for Intracellular Protein Delivery. *Adv. Drug Delivery Rev.* **2021**, No. 113837.

(11) O'Neill, C. L.; Shrimali, P. C.; Clapacs, Z. P.; Files, M. A.; Rudra, J. S. Peptide-Based Supramolecular Vaccine Systems. *Acta Biomater.* **2021**, *133*, 153−167.

(12) Sis, M. J.; Webber, M. J. Drug Delivery with Designed Peptide Assemblies. *Trends Pharmacol. Sci.* **2019**, *40* (10), 747−762.

(13) Hendricks, M. P.; Sato, K.; Palmer, L. C.; Stupp, S. I. Supramolecular Assembly of Peptide Amphiphiles. *Acc. Chem. Res.* **2017**, *50* (10), 2440−2448.

(14) Distaffen, H. E.; Jones, C. W.; Abraham, B. L.; Nilsson, B. L. Multivalent Display of Chemical Signals on Self-Assembled Peptide Scaffolds. *Pept. Sci.* **2021**, *113* (2), No. e24224.

(15) Chow, L. W.; Wang, L. j.; Kaufman, D. B.; Stupp, S. I. Self-Assembling Nanostructures to Deliver Angiogenic Factors to Pancreatic Islets. *Biomaterials* **2010**, *31* (24), 6154−6161.

(16) Anderson, C. F.; Wang, Q.; Stern, D.; Leonard, E. K.; Sun, B.; Fergie, K. J.; Choi, C. y.; Spangler, J. B.; Villano, J.; Pekosz, A.; Brayton, C. F.; Jia, H.; Cui, H. Supramolecular Filaments for Concurrent ACE2 Docking and Enzymatic Activity Silencing Enable Coronavirus Capture and Infection Prevention. *Matter* **2023**, *6* (2), 583−604.

(17) Li, Y.; Lock, L. L.; Mills, J.; Ou, B. S.; Morrow, M.; Stern, D.; Wang, H.; Anderson, C. F.; Xu, X.; Ghose, S.; Li, Z. J.; Cui, H. Selective Capture and Recovery of Monoclonal Antibodies by Self-Assembling Supramolecular Polymers of High Affinity for Protein Binding. *Nano Lett.* **2020**, *20* (10), 6957−6965.

(18) Votaw, N. L.; Collier, L.; Curvino, E. J.; Wu, Y.; Fries, C. N.; Ojeda, M. T.; Collier, J. H. Randomized Peptide Assemblies for Enhancing Immune Responses to Nanomaterials. *Biomaterials* **2021**, *273* (April), No. 120825.

(19) Rudra, J. S.; Sun, T.; Bird, K. C.; Daniels, M. D.; Gasiorowski, J. Z.; Chong, A. S.; Collier, J. H. Modulating Adaptive Immune Responses to Peptide Self-Assemblies. *ACS Nano* **2012**, *6* (2), 1557−1564.

(20) Wu, Y.; Kelly, S. H.; Sanchez-Perez, L.; Sampson, J. H.; Collier, J. H. Comparative Study of α-Helical and β-Sheet Self-Assembled Peptide Nanofiber Vaccine Platforms: Influence of Integrated T-Cell Epitopes. *Biomater. Sci.* **2020**, *8* (12), 3522−3535.

(21) Wen, Y.; Waltman, A.; Han, H.; Collier, J. H. Switching the Immunogenicity of Peptide Assemblies Using Surface Properties. *ACS Nano* **2016**, *10* (10), 9274−9286.

(22) Khan, S.; Sur, S.; Dankers, P. Y. W.; Da Silva, R. M. P.; Boekhoven, J.; Poor, T. A.; Stupp, S. I. Post-Assembly Functionalization of Supramolecular Nanostructures with Bioactive Peptides and Fluorescent Proteins by Native Chemical Ligation. *Bioconjugate Chem.* **2014**, *25* (4), 707−717.

(23) Hudalla, G. A.; Modica, J. A.; Tian, Y. F.; Rudra, J. S.; Chong, A. S.; Sun, T.; Mrksich, M.; Collier, J. H. A Self-Adjuvanting Supramolecular Vaccine Carrying a Folded Protein Antigen. *Adv. Healthc. Mater.* **2013**, *2* (8), 1114−1119.

(24) DiMaio, J. T. M.; Raymond, D. M.; Nilsson, B. L. Display of Functional Proteins on Supramolecular Peptide Nanofibrils Using a Split-Protein Strategy. *Org. Biomol. Chem.* **2017**, *15* (25), 5279−5283.

(25) Collier, J. H.; Messersmith, P. B. Enzymatic Modification of Self-Assembled Peptide Structures with Tissue Transglutaminase. *Bioconjugate Chem.* **2003**, *14* (4), 748−755.
(26) Wakabayashi, R.; Suehiro, A.; Goto, M.; Kamiya, N. Designer Aromatic Peptide Amphiphiles for Self-Assembly and Enzymatic Display of Proteins with Morphology Control. *Chem. Commun.* **2019**, *55* (5), 640−643.
(27) Wakabayashi, R.; Higuchi, A.; Obayashi, H.; Goto, M.; Kamiya, N. Ph-Responsive Self-Assembly of Designer Aromatic Peptide Amphiphiles and Enzymatic Post-Modification of Assembled Structures. *Int. J. Mol. Sci.* **2021**, *22* (7), 3459.
(28) Chen, J. L.; Fries, C. N.; Berendam, S. J.; Rodgers, N. S.; Roe, E. F.; Wu, Y.; Hang Li, S.; Jain, R.; Watts, B.; Eudailey, J.; Barfield, R.; Chan, C.; Moody, M. A.; Saunders, K. O.; Pollara, J.; Permar, S. R.; Collier, J. H.; Fouda, G. G. Self-Assembling Peptide Nanofiber HIV Vaccine Elicits Robust Vaccine-Induced Antibody Functions and Modulates Fc Glycosylation. *Sci. Adv.* **2022**, *8* (38), No. eabq0273.
(29) Strop, P. Versatility of Microbial Transglutaminase. *Bioconjugate Chem.* **2014**, *25* (5), 855−862.
(30) Ma, M.; Kuang, Y.; Gao, Y.; Zhang, Y.; Gao, P.; Xu, B. Aromatic-Aromatic Interactions Induce the Self-Assembly of Pentapeptidic Derivatives in Water to Form Nanofibers and Supramolecular Hydrogels. *J. Am. Chem. Soc.* **2010**, *132* (8), 2719−2728.
(31) Fleming, S.; Ulijn, R. V. Design of Nanostructures Based on Aromatic Peptide Amphiphiles. *Chem. Soc. Rev.* **2014**, *43* (23), 8150−8177.
(32) Tovar, J. D.; Claussen, R. C.; Stupp, S. I. Probing the Interior of Peptide Amphiphile Supramolecular Aggregates. *J. Am. Chem. Soc.* **2005**, *127* (20), 7337−7345.
(33) Takeuchi, T.; Kosuge, M.; Tadokoro, A.; Sugiura, Y.; Nishi, M.; Kawata, M.; Sakai, N.; Matile, S.; Futaki, S. Direct and Rapid Cytosolic Delivery Using Cell-Penetrating Peptides Mediated by Pyrenebutyrate. *ACS Chem. Biol.* **2006**, *1* (5), 299−303.
(34) Kim, I.; Bang, W. Y.; Kim, S.; Jin, S. M.; Hyun, J. Y.; Han, E. H.; Lee, E. Peroxisome-Targeted Supramolecular Nanoprobes Assembled with Pyrene-Labelled Peptide Amphiphiles. *Chem. - An Asian J.* **2018**, *13* (22), 3485−3490.
(35) Jeena, M. T.; Jeong, K.; Go, E. M.; Cho, Y.; Lee, S.; Jin, S.; Hwang, S. W.; Jang, J. H.; Kang, C. S.; Bang, W. Y.; Lee, E.; Kwak, S. K.; Kim, S.; Ryu, J. H. Heterochiral Assembly of Amphiphilic Peptides Inside the Mitochondria for Supramolecular Cancer Therapeutics. *ACS Nano* **2019**, *13* (10), 11022−11033.
(36) Kaur, H.; Roy, S. Enzyme-Induced Supramolecular Order in Pyrene Dipeptide Hydrogels for the Development of an Efficient Energy-Transfer Template. *Biomacromolecules* **2021**, *22*, 2393.
(37) Abe, H.; Goto, M.; Kamiya, N. Protein Lipidation Catalyzed by Microbial Transglutaminase. *Chem. - A Eur. J.* **2011**, *17* (50), 14004−14008.
(38) HogenEsch, H. Mechanism of Immunopotentiation and Safety of Aluminum Adjuvants. *Front. Immunol.* **2013**, *3* (JAN), 1−13.
(39) Higuchi, A.; Wakabayashi, R.; Kawamura, I.; Goto, M.; Kamiya, N. Influence of Self-Assembling Nonsubstrates on the Enzymatic Postmodification of Peptide Supramolecules. *Chem. Lett.* **2025**, *54* (1), 1−5.
(40) Kubota, R.; Nakamura, K.; Torigoe, S.; Hamachi, I. The Power of Confocal Laser Scanning Microscopy in Supramolecular Chemistry: In Situ Real-time Imaging of Stimuli-Responsive Multicomponent Supramolecular Hydrogels. *ChemistryOpen* **2020**, *9* (1), 67−79.
(41) Wu, Y. X.; Zhang, X. B.; Li, J. Bin; Zhang, C. C.; Liang, H.; Mao, G. J.; Zhou, L. Y.; Tan, W.; Yu, R. Q. Bispyrene-Fluorescein Hybrid Based FRET Cassette: A Convenient Platform toward Ratiometric Time-Resolved Probe for Bioanalytical Applications. *Anal. Chem.* **2014**, *86* (20), 10389−10396.
(42) Jain, R.; Pal, V. K.; Roy, S. Triggering Supramolecular Hydrogelation Using a Protein-Peptide Coassembly Approach. *Biomacromolecules* **2020**, *21* (10), 4180−4193.
(43) Rudra, J. S.; Tian, Y. F.; Jung, J. P.; Collier, J. H. A Self-Assembling Peptide Acting as an Immune Adjuvant. *Proc. Natl. Acad. Sci. U. S. A.* **2010**, *107* (2), 622−627.
(44) Chang, R.; Yan, X. Supramolecular Immunotherapy of Cancer Based on the Self-Assembling Peptide Design. *Small Struct.* **2020**, *1* (2), 2000068.
(45) Wang, H.; Luo, Z.; Wang, Y.; He, T.; Yang, C.; Ren, C.; Ma, L.; Gong, C.; Li, X.; Yang, Z. Enzyme-Catalyzed Formation of Supramolecular Hydrogels as Promising Vaccine Adjuvants. *Adv. Funct. Mater.* **2016**, *26* (11), 1822−1829.
(46) Hudalla, G. A.; Sun, T.; Gasiorowski, J. Z.; Han, H.; Tian, Y. F.; Chong, A. S.; Collier, J. H. Gradated Assembly of Multiple Proteins into Supramolecular Nanomaterials. *Nat. Mater.* **2014**, *13* (8), 829−836.
(47) Black, M.; Trent, A.; Kostenko, Y.; Lee, J. S.; Olive, C.; Tirrell, M. Self-Assembled Peptide Amphiphile Micelles Containing a Cytotoxic T-Cell Epitope Promote a Protective Immune Response in Vivo. *Adv. Mater.* **2012**, *24* (28), 3845−3849.
(48) Higuchi, A.; Som, A.; Wakabayashi, R.; Goto, M.; Kamiya, N.; Besenius, P. The Impact of Single Amino Acid Insertion on the Supramolecular Assembly Pathway of Aromatic Peptide Amphiphiles. *Chem. - Eur. J.* **2025**, No. 202404233.
(49) Sato, R.; Minamihata, K.; Ariyoshi, R.; Taniguchi, H.; Kamiya, N. Recombinant Production of Active Microbial Transglutaminase in E. Coli by Using Self-Cleavable Zymogen with Mutated Propeptide. *Protein Expr. Purif.* **2020**, *176*, No. 105730.

https://doi.org/10.1021/acsami.5c10222
ACS Appl. Mater. Interfaces 2025, 17, 44240−44248